ACS OMEGA

http://pubs.acs.org/journal/acsodf

Article

Effect of Operating Parameters on Oxidation Characteristics of Soot under the Synergistic Action of Soluble Organic Fractions and Ash

Ping Pu, Jia Fang,* Qian Zhang, Yi Yang, Zihan Qin, Zhongwei Meng, and Suozhu Pan

Cite This: *ACS Omega* 2021, 6, 17372−17378

Read Online

ACCESS | Metrics & More | Article Recommendations

ABSTRACT: Diesel particulate filter is used to reduce particulate matter (PM) emission due to the stringent emission standards. The accumulated PM has been oxidized by the periodical regeneration method to avoid pressure buildup. The innovation of this study is to explore the oxidation performance of Printex-U (PU), which is mixed with ash and soluble organic fractions, under different operating conditions. Different aspects of operating parameters, such as the oxygen ratio in an O_2/N_2 atmosphere, total flow rate, initial PU mass, and heating rate, on PU oxidation properties have been critically discussed using a thermogravimetric analyzer. The oxygen ratio in the O_2/N_2 atmosphere is positively correlated with the oxidation characteristics of PU. The comprehensive oxidation index (S) of PU under the 20% O_2/80% N_2 atmosphere increases by 184% compared with the 10% O_2/90% N_2 atmosphere. When the initial PU mass is 3 mg, the combustion stability coefficient (R_w) and S reach the best values, which are 55.53×10^5 and 2.03×10^7 $\%^2 min^{-2} {}^\circ C^{-3}$, respectively. With the increase in the heating rate, the oxidation properties of PU become sensible and deflagration occurs easily, so that 10 °C/min heating rate is the best option. This study provides a theoretical basis for the optimization design of diesel particulates during the regeneration process.

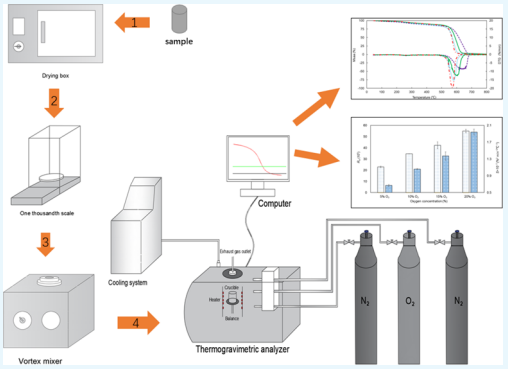

1. INTRODUCTION

In the last decades, diesel engines have attracted increasing interests from vehicle producers and the public due to their higher thermal efficiency, less carbon monoxides, and unburned hydrocarbon emissions compared with gasoline engines.[1−4] Seventy percent of commercial highway freight vehicles are diesel vehicles, which accounts for 20% of total greenhouse gas emissions.[5] Many studies have classified diesel emissions into four categories, including nitrogen oxides (NO, NO_2, N_2O, etc.), particulate matter (PM) (dry soot smoke, soluble organic fraction, ash, sulfate, etc.),[6,7] carbon monoxide, and unburned hydrocarbons.[8−11] Environmental issues pose huge threats to public health, particularly the damage caused by small-diameter PM.[12−16] Short-term or long-term exposure to PM instigates adverse health effects upon the cardiovascular (CV) system[17] and cancer.[14]

Diesel particulate filtering (DPF) are considered one of the most efficient technologies in removing diesel engine PM. DPF have been widely used in after-treatment systems.[2,3,18−21] However, DPF capturing PM for a long time will lead to lower capture efficiency and the blockage of the DPF and the increase in exhaust backpressure, thus affecting the normal operations of the engine.[22−24] There are two main types of regeneration methods of the DPF, the active regeneration and passive regeneration method.[19,25,26] Many research results show that the maximum exhaust temperature of a diesel engine is about 400 °C, which is lower than the ignition temperature of PU without a catalyst about 550−600 °C.[27,28] The ignition temperature of soot is closely related to the oxidation performance of soot.

Many operating factors affect the oxidation performance, such as the oxygen ratio in the O_2/N_2 atmosphere, heating rate,[28] contents of soluble organic fractions (SOF), species and concentrations of the catalyst,[29] type and content of ash,[24] and optimal initial sample mass.[30,31] Liang et al. found out the impact of lubricant-derived ash on the oxidation performance of soot and concluded that the ash can accelerate the oxidation of soot.[32] Meng et al. studied the oxidation behavior of soot at different heating rate, and the results have shown that the activation energy of the soot reaction decreases and the reaction rate increases with the increase in the heating rate.[28] Liang et al. revealed the effect of lube base oil on the oxidation activity of diesel soot. The disordered nanostructure of soot accelerates the oxidation of phosphorus soot.[33] Fang et al.

Received: March 23, 2021
Accepted: June 21, 2021
Published: June 28, 2021

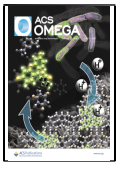

applied a thermogravimetric analyzer (TGA) to study the influence of different ash types on the oxidation performance of soot and indicated that the PU/ZnO mixture has the maximum comprehensive oxidation index (S) compared with PU/Al_2O_3 and PU/MgO mixtures.[34] Furthermore, Zhang et al. used a thermogravimetric analyzer to study the interaction effect of SOF and ash on diesel soot oxidation, and the result shows that the mass ratio of PU/ZnO/15 W at 1/1/0.1 has a best combustion performance under an O_2/N_2 atmosphere.[24] Soot oxidation characteristics are studied from the aspects of ash content, type of lubricating oil, the microstructure of soot, catalyst, and different operating parameters. The oxidation performance of soot under different synergistic conditions is not explored. Therefore, it is necessary to explore the oxidation performance of soot under the combined action of various factors, which can provide a theoretical basis for the diesel exhaust after-treatment process.

The innovation of this study is to explore the oxidation performance of soot, which is mixed with ash and SOF, under different operating conditions. This research aims to provide detailed information under the synergistic effects of ash and SOF on the effect of the (1) oxygen ratio in an O_2/N_2 atmosphere, (2) total flow rate, (3) initial PU combustion mass, and (4) heating rate on soot oxidation performance in an O_2/N_2 atmosphere.

2. EXPERIMENTAL APPARATUS AND MATERIAL

The influence of operating parameters on soot oxidation performance of soot under the synergistic action of ash and 15 W lubricating oil has been studied by using a TGA (TG209F3 from NETZSCH, Germany), and the main parameters of the TGA are listed in Table 1. The properties of real diesel particle

Table 1. Main Parameters of Types TG209F3

parameters	value
balance sensitivity (μg)	0.1
heating rate (°C/min)	0.001−100
range of temperature (°C)	45−1000
size of the crucible (mm)	Φ 6.8
measuring dynamic range (g)	0−2

soot are affected by engine working conditions, so they are very difficult to obtain.[35] PU has a similar microstructure to soot and the reactivity of PU follows the same trend as diesel soot,[29,36] so it is widely used to replace diesel particulates.[10,29,37−39] In this study, diesel soot is replaced by PU (Degussa GmbH, Frankfurt, Germany), and the physical properties are given in Table 2. The characteristic parameters

Table 2. Physical Properties of PU

soot	diameter (nm)	BET (m^2/g)	oil absorption (g/100 g)	ash content (%)
PU	25	92	460	0.02

of ZnO ash (nanoparticles are purchased from Shanghai Aladdin Biochemical, China) are summarized in Table 3. The experimental bench is shown in Figure 1.

3. EXPERIMENTAL METHOD AND DATA ANALYSIS

The influence of operating parameters, such as the oxygen ratio in the O_2/N_2 atmosphere, total flow rate, the initial PU mass of

Table 3. Physical Properties of Ashes

ash	particle diameter (nm)	metal's basis
ZnO	50 ± 10	99.8%

combustion, and heating ramp on soot oxidation performance under the synergistic effect of ZnO ash and SOF (15 W lubricating oil[32]) are investigated, and the mixing mass ratio for PU/ZnO/15 W is 1/1/0.1. A vacuum drying chamber is set at 110 °C to dry the samples for 1 h. PU particles are in a tight contact mode with the catalyst and SOF in many studies.[32,35,40] To make the sample in tight contact, the experiment uses a vortex oscillator to mix the sample in a certain proportion for 15 min. In each experiment, the mixture is transferred to an alumina crucible with an inner diameter of 6.8 mm and a height of 7.4 mm and heated from 45 to 800 °C.

The controlled variable method has been used in this experiment to study the effects of different operating parameters on the oxidation performance of soot. The experiment is divided into four groups, and the operating parameters of the four groups are as follows. (1) Four oxygen concentrations have been tested, which include 5, 10, 15, and 20% O_2 in O_2/N_2 atmosphere experiments. The total flow rate, the initial PU mass, and the heating ramp is 100 mL/min, 3 mg, and 10 °C/min, respectively. (2) Five total flow rates have been tested, which include 80, 90, 100, 110, and 120 mL/min. The oxygen concentration, the initial PU mass, and the heating ramp is 20%, 3 mg, and 10 °C/min, respectively. (3) Five initial PU masses have been tested, which include 2, 3, 4, 5, 7, and 9 mg. The oxygen concentration, the total flow rate, and the heating ramp are 20%, 100 mL/min, and 10 °C/min, respectively. (4) Five heating rates have been tested, which include 10, 20, 30, 40, and 50 °C/min. Five initial PU masses have been tested, which include 2, 3, 4, 5, 7, and 9 mg. The oxygen concentration, the total flow rate, and the initial PU mass are 20%, 100 mL/min, and 3 mg, respectively. Each test is running in duplicate and the ± error indicates the standard deviation of the two results.

4. DATA ANALYSIS

The change line of the sample mass with temperature is defined as a thermogravimetric (TG) curve in Figure 2, which is obtained by a TGA. The DTG curve is the derivative of the TG curve. To better represent and evaluate the oxidation characteristics of particles, the combustion start temperature (T_s), peak temperature (T_p), and end temperature (T_e) are defined in Figure 2, respectively.[34,39,41] T_p represents the corresponding temperature to the peak of the DTG outline, which represents W_{max}. The average value of the mass loss rate from the beginning of the reaction to the end is W_{mean}. T_s is the point where the sample begins to burn, and T_e is defined as the temperature when the elementary combustion process is realized. T_s, T_p, and T_e are obtained as follows. T_p is the intersection of the abscissa and the vertical line across the peak point A of the DTG curves, which crosses the point B on the TG curves. The blue line is tangent to the TG curves passing through B. T_s is the temperature at point C, which is the blue line across the horizontal line whose ordinate is 100%. T_e is the temperature at point D, which is the blue line across DTG curves.

The S and the combustion stability index (R_w) include the ease of ignition, the firing velocity, and the end and peak temperature. S reflects the ignition, combustion, and burnout

https://doi.org/10.1021/acsomega.1c01537
ACS Omega 2021, 6, 17372−17378

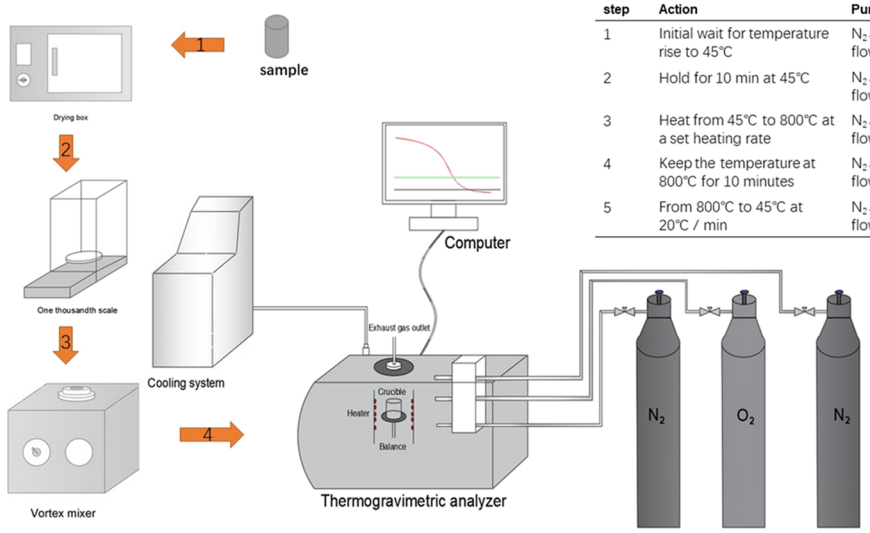

Table TGA program

step	Action	Purge gas
1	Initial wait for temperature rise to 45℃	N_2、O_2, at set flow rate
2	Hold for 10 min at 45℃	N_2、O_2, at set flow rate
3	Heat from 45℃ to 800℃ at a set heating rate	N_2、O_2, at set flow rate
4	Keep the temperature at 800℃ for 10 minutes	N_2、O_2, at set flow rate
5	From 800℃ to 45℃ at 20℃ / min	N_2、O_2, at set flow rate

Figure 1. Experimental bench diagram.

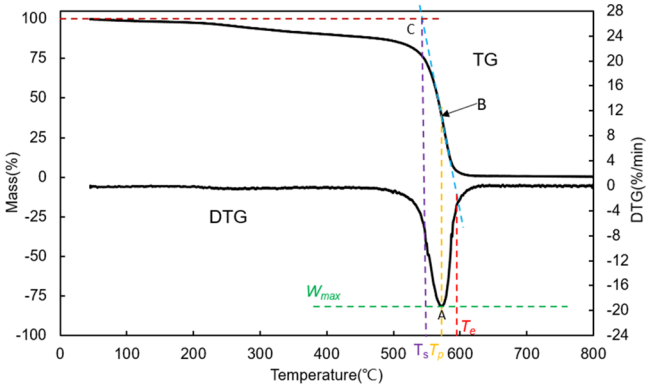

Figure 2. Definition of the combustion characteristic temperature with the TG-DTG tangent method.

properties of a sample and it can be used to evaluate the oxidation property of the sample.[41−44] R_w represents the stability in the process of sample combustion.[24,45] With the increase in S and R_w, the combustion process improves. S and R_w are, respectively, defined as following:

$$S = \frac{W_{max} \times W_{mean}}{T_s^2 \times T_e} \quad (1)$$

$$R_w = 8.5875 \times 10^7 \times \frac{W_{max}}{T_s \times T_p} \quad (2)$$

where W_{max} and W_{mean} represent the maximum mass loss rate and average mass loss rate, respectively. T_s, T_p, and T_e represent the combustion start temperature, the combustion peak temperature, and the combustion end temperature, respectively.

5. RESULTS AND DISCUSSION

5.1. Influence of the Oxygen Ratio in an O_2/N_2 Atmosphere on Soot Oxidation. The oxygen present in a diesel engine exhaust is between 5 and 18%,[22,31,46] and it can reach 20% in a large load.[14] As a result, 5% O_2, 10% O_2, 15% O_2, and 20% O_2 are taken to investigate the effect of oxygen concentration on the oxidation characteristics of PU. The TG-DTG curves of the PU/ZnO/15 W mixture at different oxygen ratios in O_2/N_2 atmospheres are displayed in Figure 3. The

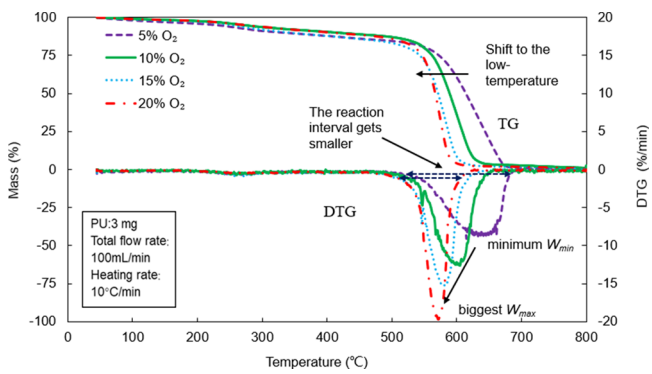

Figure 3. TG-DTG curves at different oxygen ratios in O_2/N_2 atmospheres.

oxidation properties of PU became better with the increase in the oxygen ratio, which is consistent with the result of Shi et al.[47] Their results show that increasing the oxygen volume fraction promotes the reaction between coal and oxygen. TG-DTG curves and the inflection point shift to the low-temperature region, and the oxidation reaction range of PU, T_p, and T_e gradually decreases with the increase in the oxygen ratio in the O_2/N_2 atmosphere. The reason for this phenomenon is that the reaction has more diffusion of oxygen atoms with the increase in the oxygen ratio.[42] With the increase in the oxygen ratio in the O_2/N_2 atmosphere, PU can fully come in contact with oxygen molecules and quickly react.

Figure 4 shows that R_w and S increase with the oxygen ratio in the O_2/N_2 atmosphere. With the increase in the oxygen ratio in the O_2/N_2 atmosphere, T_e and T_p decrease, while W_{max} and W_{mean} increase. At a 20% oxygen ratio in the O_2/N_2 atmosphere, R_w and S reach the largest values at 56.43×10^5 and 2.04×10^7 $\%^2 min^{-2} \circ C^{-3}$, respectively (Table 4). The reason for this phenomenon can be explained as follows: (1) A higher oxygen ratio will allow more sufficient diffusion of oxygen;[48] (2) with the increase in the oxygen ratio, more oxygen can be absorbed by the active structure of PU. To sum

https://doi.org/10.1021/acsomega.1c01537
ACS Omega 2021, 6, 17372−17378

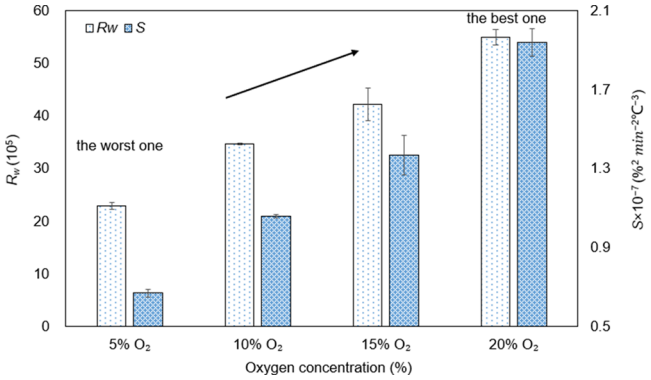

Figure 4. Comparison of S and R_w at different oxygen ratios in O_2/N_2 atmospheres.

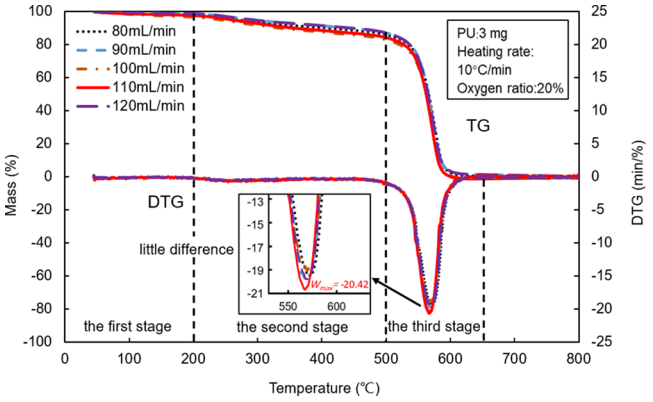

Figure 5. TG-DTG curves with different total flow rates.

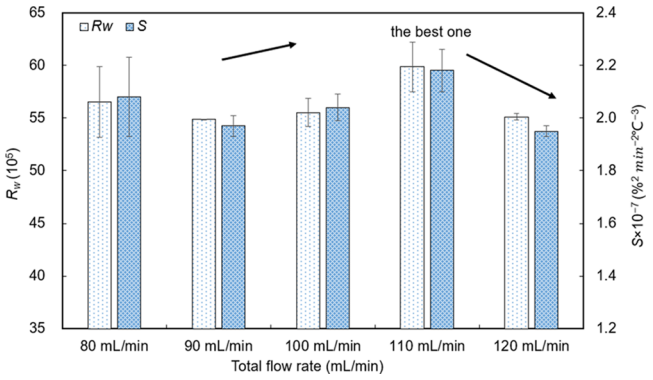

Figure 6. Comparison of S and R_w at different total flow rates.

up, the increase in the oxygen ratio in the O_2/N_2 atmosphere promotes the oxidation regeneration of PU and makes TG-DTG curves move to the direction of the low-temperature zone, and it reduces T_e and T_p and increases R_w and S.

5.2. Influence of the Total Flow Rate on Soot Oxidation. Figure 5 shows the change of soot oxidation characteristics at different total flow rates (80, 90, 100, 110, and 120 mL/min). It can be seen from Figure 5 that the oxidation process of soot can be divided into three stages: 45−200 °C, 200−500 °C, and 500−650 °C. The first-order TG curves decrease by about 5%, which is due to the evaporation of water in the sample.[34] The second stage shows a slow decline at about 10%, because volatile components such as SOF are broken down. The oxidation reaction of soot mainly occurs in the third stage, and the sample reacts rapidly with the increase in temperature.

Figures 5 and 6 represent that the total flow rate has little influence on the oxidation characteristics of soot. The change in the total flow rate is too small to cause an obvious increase in the number of oxygen molecules in the O_2/N_2 atmosphere, which cannot make an obvious difference of S and R_w at different total flow rates. Comparatively speaking, the values of S and R_w reach the highest values at a 110 mL/min total flow rate. The oxidation reaction of soot is the most stable at the 110 mL/min total gas flow, so 110 mL/min has been selected as the operating parameter for the next set of experiments.

5.3. Influence of the Initial PU Combustion Mass on Soot Oxidation. Figures 7 and 8, respectively, display the TG-DTG curves, the change of S and R_w under different initial

Table 4. Summary of Characteristic Parameters in All the Cases of This Study

case	operating parameters	T_s (°C)	T_e (°C)	T_p (°C)	W_{max} (%/min)	W_{mean} (%/min)	Rw (10^5)	$S \times 10^7$ $\%^2 min^{-2}$ ° C^{-3}
1−2	5%O_2	557 ± 2	678 ± 1	611 ± 4	9.35 ± 0.25	1.56 ± 0.02	23.55 ± 0.65	0.69 ± 0.02
3−4	10% O_2	545 ± 2	641 ± 1	599 ± 6	12.8 ± 0.11	1.57 ± 0.03	33.70 ± 0.11	1.05 ± 0.01
5−6	15% O_2	538 ± 5	611 ± 9	580 ± 1	16.4 ± 1.31	1.38 ± 0.20	45.31 ± 3.07	1.27 ± 0.10
7−8	20% O_2	542 ± 2	590 ± 5	568 ± 6	20.2 ± 0.51	1.74 ± 0.03	56.43 ± 1.52	2.04 ± 0.07
9−10	80 mL/min	540 ± 1	593 ± 3	569 ± 3	20.2 ± 0.87	1.78 ± 0.50	56.53 ± 3.35	2.08 ± 0.15
11−12	90 mL/min	540 ± 4	594 ± 3	568 ± 1	19.5 ± 0.15	1.74 ± 0.02	54.86 ± 0.03	1.97 ± 0.04
13−14	100 mL/min	541 ± 2	591 ± 1	567 ± 1	19.6 ± 0.94	1.76 ± 0.02	55.53 ± 2.35	2.04 ± 0.08
15−16	110 mL/min	536 ± 3	592 ± 3	569 ± 1	21.1 ± 0.58	1.79 ± 0.01	59.09 ± 1.33	2.18 ± 0.05
17−18	120 mL/min	540 ± 1	593 ± 3	568 ± 2	19.6 ± 0.02	1.72 ± 0.01	55.11 ± 0.29	1.95 ± 0.02
19−20	PU 2 mg	540 ± 3	594 ± 2	567 ± 3	19.4 ± 0.38	1.72 ± 0.03	53.08 ± 0.41	1.92 ± 0.05
21−22	PU 3 mg	536 ± 4	591 ± 1	567 ± 1	19.6 ± 0.94	1.76 ± 0.02	55.53 ± 2.35	2.03 ± 0.09
23−24	PU 4 mg	537 ± 1	593 ± 1	567 ± 1	17.8 ± 0.30	1.77 ± 0.01	50.35 ± 1.76	1.85 ± 0.07
25−26	PU 5 mg	529 ± 1	591 ± 1	564 ± 1	15.4 ± 1.22	1.78 ± 0.03	44.43 ± 2.35	1.66 ± 0.12
27−28	PU 7 mg	505 ± 7	595 ± 0	564 ± 2	12.7 ± 0.47	1.79 ± 0.20	38.31 ± 0.77	1.50 ± 0.02
29−30	PU 9 mg	501 ± 12	604 ± 3	570 ± 5	10.3 ± 0.71	1.72 ± 0.01	31.02 ± 1.15	1.17 ± 0.01
31−32	10 °C/min	540 ± 1	589 ± 3	566 ± 1	20.6 ± 0.04	1.78 ± 0.00	58.16 ± 0.28	2.14 ± 0.02
33−34	20 °C/min	550 ± 4	633 ± 0	605 ± 1	26.5 ± 0.35	3.30 ± 0.00	67.86 ± 0.29	4.49 ± 0.02
35−36	30 °C/min	549 ± 1	659 ± 3	621 ± 1	27.8 ± 1.05	4.74 ± 0.03	71.22 ± 3.07	6.88 ± 0.38
37−38	40 °C/min	554 ± 4	689 ± 3	646 ± 1	31.5 ± 0.36	6.01 ± 0.01	78.87 ± 0.18	8.99 ± 0.01
39−40	50 °C/min	571 ± 7	706 ± 2	660 ± 3	37.7 ± 0.34	7.42 ± 0.09	86.03 ± 0.73	10.21 ± 0.04

https://doi.org/10.1021/acsomega.1c01537
ACS Omega 2021, 6, 17372−17378

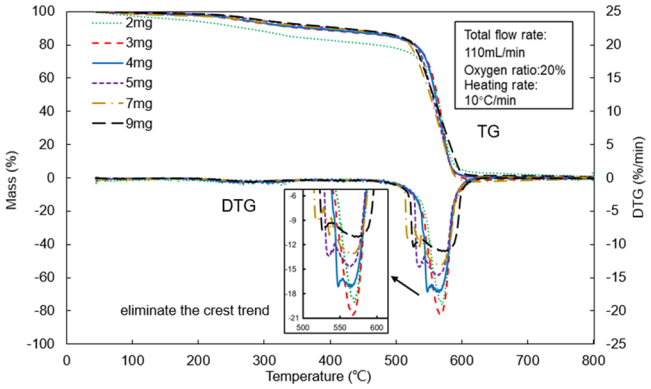

Figure 7. TG-DTG curves at different initial PU combustion masses.

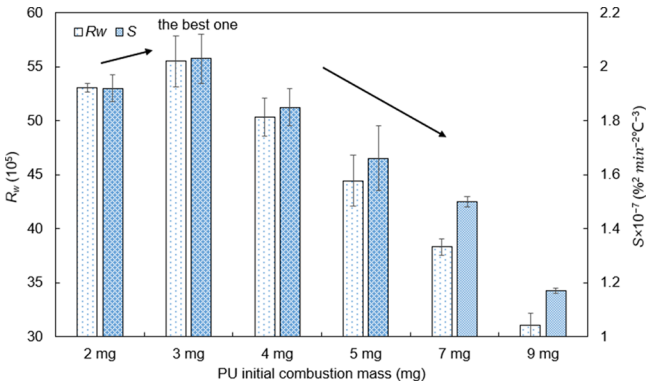

Figure 8. Comparison of S and R_w at different initial PU combustion masses.

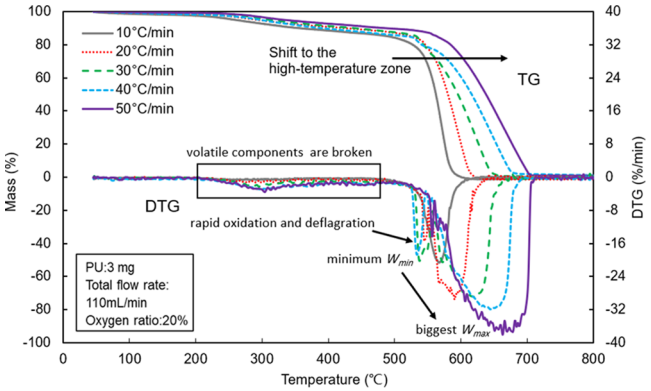

Figure 9. TG-DTG curves at different heating rates.

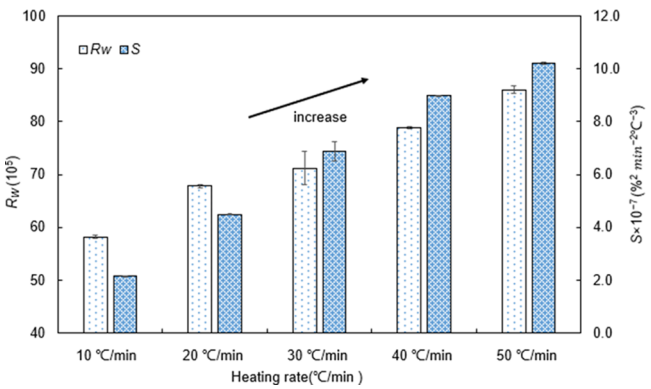

Figure 10. Comparison of S and R_w at different heating rates.

combustion masses (2, 3, 4, 5, 7, and 9 mg) of PU. The peak value of the curves of the mass loss rate moderately increases first and then decreases, reaching a maximum value of 19.69%/min at 3 mg, as shown in Figure 7. DTG curves show a trend of decreaking gradually with the increase in the added PU mass, which is a sign of deterioration of the oxidation reaction. It can be seen from the figure that with the increase in the initial combustion mass of PU, the TG-DTG curves migrate to the low-temperature zone. Meanwhile, R_w and S slowly decrease first and then increase. When the initial mass of PU is 3 mg, the largest value of R_w and S reached are 55.53×10^5 and 2.03×10^7 $\%^2 min^{-2} \circ C^{-3}$, respectively. The possible reason is that oxygen diffusion and total oxygen has been limited. The heat transfer of the sample in the crucible is mainly affected by three kinds of mass transfer resistance.[48] The heat transfer and the oxidation reaction of soot become worse when the mass of the initial PU increases. The initial combustion of PU mass in 3 mg has the most stable thermogravimetric laboratory selection.

5.4. Influence of the Heating Rate on Soot Oxidation.

Figures 9 and 10 display the oxidation characteristics of PU at different heating rates. TG-DTG curves shift to the high-temperature region with the increase in the heating rate, as shown in Figure 9. The fluctuation range, which is the decomposition of volatile components at the low-temperature zone, increases when the heating rate increases. The reasons for this phenomenon are heat-transfer lag and react lag. The increase of the heating rate makes the temperature difference larger between the actual sample temperature and the temperature displayed by the TGA, and the heat-transfer time becomes shorter. The residence time of the sample at the set temperature has been reduced when the heating rate increases. However, the oxidized reaction of the sample needs fixed times. Before the sample is fully reacted, the temperature displayed by the TGA rises to a higher level, which makes the reaction curves shift to the high-temperature region as a whole.

When the heating rate increases, more energy is injected into this reaction, which causes rapid oxidation and deflagration. The increase in the characteristic temperature is not as much as that of W_{max} and W_{mean}, which makes S and R_w increase. As seen from Figure 9, the reaction lag and heat-transfer lag have a great impact on the oxidation of soot. Kinetic data can be extracted from thermal experiments only when the reaction is avoided to the diffusive-controlled state.[49] From this perspective, a low sample mass is preferred through assuring the accuracy and repeatability of the results, which is consistent with Rodriguez-Fernández and Vázquez's conclusions.[50]

6. CONCLUSIONS

This research aims to provide detailed information under the influence of operating parameters including the oxygen ratio in an O_2/N_2 atmosphere, total flow rate, initial PU combustion mass, and heating rate on soot oxidation performance in an O_2/N_2 atmosphere. The following conclusions are obtained from the above experimental results.

(1) With the increase in the oxygen ratio in the O_2/N_2 atmosphere, TG-DTG curves move toward the low-temperature region.

(2) The total flow rate has little effect on the oxidation performance of soot. When the total flow rate is 110 mL/min, the maximum R_w and S are 59.09×10^5 and 2.18×10^7 $\%^2 min^{-2} \circ C^{-3}$, respectively.

https://doi.org/10.1021/acsomega.1c01537
ACS Omega 2021, 6, 17372−17378

(3) The reaction shifts to the low-temperature zone with the increase in the initial PU combustion mass. R_w and S increase slowly at first and then decrease and reach the maximum values of 55.53×10^5 and 2.03×10^7 $\%^2 min^{-2} {}^\circ C^{-3}$ at 3 mg, respectively.

(4) TG-DTG curves shift to the high-temperature region and W_{max}, W_{mean}, R_w, and S increase when the heating rate increases. A 10 °C/min heating rate is the best option in this study.

AUTHOR INFORMATION

Corresponding Author

Jia Fang − *Key Laboratory of Fluid and Power Machinery, Ministry of Education, School of Energy and Power Engineering and Vehicle Measurement, Control and Safety Key Laboratory of Sichuan Province, School of Automobile and Transportation, Xihua University, Chengdu 610039, PR China;* orcid.org/0000-0002-0696-8958; Phone: +8628 87726799; Email: jiafang@mail.xhu.edu.cn

Authors

Ping Pu − *Vehicle Measurement, Control and Safety Key Laboratory of Sichuan Province, School of Automobile and Transportation, Xihua University, Chengdu 610039, PR China*

Qian Zhang − *Vehicle Measurement, Control and Safety Key Laboratory of Sichuan Province, School of Automobile and Transportation, Xihua University, Chengdu 610039, PR China*

Yi Yang − *Vehicle Measurement, Control and Safety Key Laboratory of Sichuan Province, School of Automobile and Transportation, Xihua University, Chengdu 610039, PR China*

Zihan Qin − *Vehicle Measurement, Control and Safety Key Laboratory of Sichuan Province, School of Automobile and Transportation, Xihua University, Chengdu 610039, PR China;* orcid.org/0000-0002-6403-1530

Zhongwei Meng − *Key Laboratory of Fluid and Power Machinery, Ministry of Education, School of Energy and Power Engineering and Vehicle Measurement, Control and Safety Key Laboratory of Sichuan Province, School of Automobile and Transportation, Xihua University, Chengdu 610039, PR China;* orcid.org/0000-0002-0141-039X

Suozhu Pan − *Vehicle Measurement, Control and Safety Key Laboratory of Sichuan Province, School of Automobile and Transportation, Xihua University, Chengdu 610039, PR China*

Complete contact information is available at: https://pubs.acs.org/10.1021/acsomega.1c01537

Notes

The authors declare no competing financial interest.

ACKNOWLEDGMENTS

This work has been supported by (1) The National Natural Science Foundation of China (52076182); (2) Science and Technology Department of Sichuan Province (2021YJ0332, 2019YJ0394); (3) Graduate Innovation Fund of Xihua University (YCJJ2020069); (4) Young Scholars Reserve Talents Program of Xihua University; and (5) Open Research Subject of Provincial Engineering Research Center for New Energy Vehicle Intelligent Control and Simulation Test Technology of Sichuan (XNYQ2021-001).

REFERENCES

(1) Ji, L.; Cai, Y.; Shi, Y.; Fan, R.; Wang, W.; Chen, Y. Effects of Nonthermal Plasma on Microstructure and Oxidation Characteristics of Particulate Matter. *Environ. Sci. Technol.* **2020**, *54*, 2510−2519.

(2) Guan, B.; Zhan, R.; Lin, H.; Huang, Z. Review of the state-of-the-art of exhaust particulate filter technology in internal combustion engines. *J. Environ. Manage.* **2015**, *154*, 225−258.

(3) Fang, J.; Meng, Z.; Li, J.; Pu, Y.; du, Y.; Li, J.; Jin, Z.; Chen, C.; G. Chase, G. The influence of ash on soot deposition and regeneration processes in diesel particular filter. *Appl. Therm. Eng.* **2017**, *124*, 633−640.

(4) Jiaqiang, E.; Zhao, X.; Xie, L.; Zhang, B.; Chen, J.; Zuo, Q.; Han, D.; Hu, W.; Zhang, Z. Performance enhancement of microwave assisted regeneration in a wall-flow diesel particulate filter based on field synergy theory. *Energy* **2019**, *169*, 719−729.

(5) Quiros, D. C.; Smith, J.; Thiruvengadam, A.; Huai, T.; Hu, S. Greenhouse gas emissions from heavy-duty natural gas, hybrid, and conventional diesel on-road trucks during freight transport. *Atmos. Environ.* **2017**, *168*, 36−45.

(6) Collura, S.; Chaoui, N.; Azambre, B.; Finqueneisel, G.; Heintz, O.; Krzton, A.; Koch, A.; Weber, J. V. Influence of the soluble organic fraction on the thermal behaviour, texture and surface chemistry of diesel exhaust soot. *Carbon* **2005**, *43*, 605−613.

(7) Han, W.; Lu, Y.; Jin, C.; Tian, X.; Peng, Y.; Pan, S.; Liu, H.; Zhang, P.; Zhong, Y. Study on influencing factors of particle emissions from a RCCI engine with variation of premixing ratio and total cycle energy. *Energy* **2020**, *202*, No. 117707.

(8) Paustenbach, D. J.; Madl, A. K.; Donovan, E.; Clark, K.; Fehling, K.; Lee, T. C. Chrysotile asbestos exposure associated with removal of automobile exhaust systems (ca. 1945-1975) by mechanics: results of a simulation study. *J. Expo. Sci. Environ. Epidemiol.* **2006**, *16*, 156−171.

(9) Wang, F.; Zhang, H.; Liang, J.; Tang, Q.; Li, Y.; Shang, Z. High emission reduction performance of a novel organic-inorganic composite filters containing sepiolite mineral nanofibers. *Sci. Rep.* **2017**, *7*, 43218.

(10) Singer, C.; Kureti, S. Soot oxidation in diesel exhaust on manganese oxide catalyst prepared by flame spray pyrolysis. *Appl. Catal., B* **2020**, *272*, No. 118961.

(11) Han, W.; Li, B.; Pan, S.; Lu, Y.; Li, X. Combined effect of inlet pressure, total cycle energy, and start of injection on low load reactivity controlled compression ignition combustion and emission characteristics in a multi-cylinder heavy-duty engine fueled with gasoline/diesel. *Energy* **2018**, *165*, 846−858.

(12) Barregard, L.; Molnàr, P.; Jonson, J. E.; Stockfelt, L. Impact on Population Health of Baltic Shipping Emissions. *Int. J. Environ. Res. Public Health* **2019**, *16*, 1954.

(13) Lu, C.; Liu, T.; Shi, Q.; Li, Q.; Xin, Y.; Zheng, L.; Zhang, Z. Plausibility of potassium ion-exchanged ZSM-5 as soot combustion catalysts. *Sci. Rep.* **2017**, *7*, 3300.

(14) Shi, Y.; Cai, Y.; Li, X.; Ji, L.; Chen, Y.; Wang, W. Evolution of diesel particulate physicochemical properties using nonthermal plasma. *Fuel* **2019**, *253*, 1292−1299.

(15) Bensaid, S.; Marchisio, D. L.; Russo, N.; Fino, D. Experimental investigation of soot deposition in diesel particulate filters. *Catal. Today* **2009**, *147*, S295−S300.

(16) Liu, J.; Yang, J.; Sun, P.; Zhao, L.; Liu, Z. Experimental Study on Soot Oxidation Characteristics of Diesel Engine with Ce-Based Fuel-Borne Catalyst Fuel. *J. Energy Eng.* **2020**, *146*, No. 04020009.

(17) Liu, T.; Zhang, P.; Ling, Y.; Hu, G.; Gu, J.; Yang, H.; Wei, J.; Wang, A.; Jin, H. Protective Effect of Colla corii asini against Lung Injuries Induced by Intratracheal Instillation of Artificial Fine Particles in Rats. *Int. J. Mol. Sci.* **2019**, *20*, 55.

(18) Shi, Y.; Cai, Y.; Fan, R.; Cui, Y.; Chen, Y.; Ji, L. Characterization of soot inside a diesel particulate filter during a

nonthermal plasma promoted regeneration step. *Appl. Therm. Eng.* **2019**, *150*, 612−619.
(19) Deng, Y.; Wang, X.; Chen, G.; Wu, H.; Han, Z.; Li, R. Experimental Study on a Diesel Particulate Filter with Reciprocating Flow. *ACS Omega* **2019**, *4*, 17098−17108.
(20) Fang, J.; Meng, Z.; Li, J.; Du, Y.; Qin, Y.; Jiang, Y.; Bai, W.; Chase, G. G. The effect of operating parameters on regeneration characteristics and particulate emission characteristics of diesel particulate filters. *Appl. Therm. Eng.* **2019**, *148*, 860−867.
(21) Meng, Z.; Chen, C.; Li, J.; Fang, J.; Tan, J.; Qin, Y.; Jiang, Y.; Qin, Z.; Bai, W.; Liang, K. Particle emission characteristics of DPF regeneration from DPF regeneration bench and diesel engine bench measurements. *Fuel* **2020**, *262*, No. 116589.
(22) Rossomando, B.; Meloni, E.; De Falco, G.; Sirignano, M.; Arsie, I.; Palma, V. Experimental characterization of ultrafine particle emissions from a light-duty diesel engine equipped with a standard DPF. *Proc. Combust. Inst.* **2021**, *38*, 5695−5702.
(23) Grigoratos, T.; Fontaras, G.; Giechaskiel, B.; Zacharof, N. Real world emissions performance of heavy-duty Euro VI diesel vehicles. *Atmos. Environ.* **2019**, *201*, 348−359.
(24) Zhang, Q.; Fang, J.; Meng, Z.; Chen, C.; Qin, Z. Thermogravimetric analysis of soot combustion in the presence of ash and soluble organic fraction. *RSC Adv.* **2020**, *10*, 33436−33443.
(25) Huang, J.; Liu, Y.; Meng, Z.; Peng, Y.; Li, H.; Zhang, Z.; Zhang, Q.; Qin, Z.; Mao, J.; Fang, J. Effect of Different Aging Conditions on the Soot Oxidation by Thermogravimetric Analysis. *ACS Omega* **2020**, *5*, 30568.
(26) Meng, Z.; Li, J.; Fang, J.; Tan, J.; Qin, Y.; Jiang, Y.; Qin, Z.; Bai, W.; Liang, K. Experimental study on regeneration performance and particle emission characteristics of DPF with different inlet transition sections lengths. *Fuel* **2020**, *262*, No. 116487.
(27) Li, Y.; Weinstein, M.; Roth, S. NO oxidation on catalyzed soot filters. *Catal. Today* **2015**, *258*, 396−404.
(28) Meng, Z.; Yang, D.; Yan, Y. Study of carbon black oxidation behavior under different heating rates. *J. Therm. Anal. Calorim.* **2014**, *118*, 551−559.
(29) Atribak, I.; Bueno-López, A.; García-García, A. Uncatalysed and catalysed soot combustion under NO_x+O_2: Real diesel versus model soots. *Combust. Flame* **2010**, *157*, 2086−2094.
(30) Gao, J.; Ma, C.; Xing, S.; Sun, L.; Huang, L. A review of fundamental factors affecting diesel PM oxidation behaviors. *Sci. Chin. Technol. Sci.* **2018**, *61*, 330−345.
(31) Sharma, H. N.; Pahalagedara, L.; Joshi, A.; Suib, S. L.; Mhadeshwar, A. B. Experimental Study of Carbon Black and Diesel Engine Soot Oxidation Kinetics Using Thermogravimetric Analysis. *Energy Fuels* **2012**, *26*, 5613−5625.
(32) Liang, X.; Wang, Y.; Wang, K.; Wang, Y.; Zhang, H.; Zhao, B.; Lv, X. Experimental study of impact of lubricant-derived ash on oxidation reactivity of soot generated in diesel engines. *Proc. Combust. Inst.* **2021**, *38*, 5635−5642.
(33) Liang, X.; Wang, Y.; Wang, Y.; Zhao, B.; Zhang, Z.; Lv, X.; Wu, Z.; Cai, X.; Wang, K. Impact of lubricating base oil on diesel soot oxidation reactivity. *Combust. Flame* **2020**, *217*, 77−84.
(34) Fang, J.; Qin, Z.; Meng, Z.; Jiang, Y.; Liu, J.; Zhang, Q.; Tan, J. Performance of Diesel Soot Oxidation in the Presence of Ash Species. *Energy Fuels* **2020**, *34*, 2185−2192.
(35) Vernikovskaya, N. V.; Pavlova, T. L.; Mokrinskii, V. V.; Murzin, D. Y.; Chumakova, N. A.; Noskov, A. S. Soot particulates abatement in diesel engine exhaust by catalytic oxidation followed their trapping in filters. *Chem. Eng. J.* **2015**, *269*, 416−424.
(36) Setiabudi, A.; Makkee, M.; Moulijn, J. A. The role of NO_2 and O_2 in the accelerated combustion of soot in diesel exhaust gases. *Appl. Catal., B* **2004**, *50*, 185−194.
(37) Nejar, N.; Makkee, M.; Illangomez, M. Catalytic removal of NO_x and soot from diesel exhaust: Oxidation behaviour of carbon materials used as model soot. *Appl. Catal., B* **2007**, *75*, 11−16.
(38) Tighe, C. J.; Twigg, M. V.; Hayhurst, A. N.; Dennis, J. S. The kinetics of oxidation of Diesel soots and a carbon black (Printex U) by O_2 with reference to changes in both size and internal structure of the spherules during burnout. *Carbon* **2016**, *107*, 20−35.
(39) Fang, J.; Zhang, Q.; Meng, Z.; Luo, Y.; Ou, J.; Du, Y.; Zhang, Z. Effects of ash composition and ash stack heights on soot deposition and oxidation processes in catalytic diesel particulate filter. *J. Energy Inst.* **2020**, *93*, 1942−1950.
(40) Jian, S.; Yang, Y.; Ren, W.; Xing, L.; Zhao, D.; Tian, Y.; Ding, T.; Li, X. Kinetic analysis of morphologies and crystal planes of nanostructured CeO_2 catalysts on soot oxidation. *Chem. Eng. Sci.* **2020**, *226*, No. 115891.
(41) Fang, J.; Shi, R.; Meng, Z.; Jiang, Y.; Qin, Z.; Zhang, Q.; Qin, Y.; Tan, J.; Bai, W. The interaction effect of catalyst and ash on diesel soot oxidation by thermogravimetric analysis. *Fuel* **2019**, *258*, No. 116151.
(42) Wang, X.; Li, S.; Adeosun, A.; Li, Y.; Vujanović, M.; Tan, H.; Duić, N. Effect of potassium-doping and oxygen concentration on soot oxidation in O_2/CO_2 atmosphere: A kinetics study by thermogravimetric analysis. *Energy Convers. Manage.* **2017**, *149*, 686−697.
(43) Saeed, S.; Saleem, M.; Durrani, A. Thermal performance analysis and synergistic effect on co-pyrolysis of coal and sugarcane bagasse blends pretreated by trihexyltetradecylphosphonium chloride. *Fuel* **2020**, *278*, No. 118240.
(44) Munir, S.; Sattar, H.; Nadeem, A.; Azam, M. Thermal and kinetic performance analysis of corncobs, Falsa sticks, and Chamalang coal under oxidizing and inert atmospheres. *Energy Sources, Part A* **2017**, *39*, 775−782.
(45) Lang, Q.; Zhang, B.; Liu, Z.; Chen, Z.; Xia, Y.; Li, D.; Ma, J.; Gai, C. Co-hydrothermal carbonization of corn stalk and swine manure: Combustion behavior of hydrochar by thermogravimetric analysis. *Bioresour. Technol.* **2019**, *271*, 75−83.
(46) Jiaqiang, E.; Zheng, P.; Han, D.; Zhao, X.; Deng, Y. Effects analysis on soot combustion performance enhancement in a rotary diesel particulate filter unit during continuous microwave heating. *Fuel* **2020**, *276*, No. 118043.
(47) Shi, X.; Zhang, Y.; Chen, X.; Zhang, Y.; Ma, T. Numerical study on the oxidation reaction characteristics of coal under temperature-programmed conditions. *Fuel Process. Technol.* **2021**, *213*, No. 106671.
(48) Song, Q.; He, B.; Yao, Q.; Meng, Z.; Chen, C. Influence of diffusion on thermogravimetric analysis of carbon black oxidation. *Energy Fuels* **2006**, *20*, 1895−1900.
(49) Lapuerta, M.; Rodríguez-Fernández, J.; Sánchez-Valdepeñas, J. Soot reactivity analysis and implications on diesel filter regeneration. *Prog. Energy Combust. Sci.* **2020**, *78*, No. 100833.
(50) Rodríguez-Fernández, J.; Oliva, F.; Vázquez, R. A. Characterization of the Diesel Soot Oxidation Process through an Optimized Thermogravimetric Method. *Energy Fuels* **2011**, *25*, 2039−2048.

https://doi.org/10.1021/acsomega.1c01537
ACS Omega 2021, 6, 17372−17378